

DOI:10.1002/ejic.201402314

# Synthesis and Structure of $[\text{Et}_3\text{NH}][\text{Fe}(\text{HL})_2]$ [ $\text{H}_3\text{L} = \text{L-2-}$ (3,5-Di-*tert*-butyl-2-hydroxybenzylamino)succinic Acid] and Its Catalytic Activity towards Efficient Photodegradation of Dyes in the Presence of $\text{H}_2\text{O}_2$

Sohaham Dasgupta,<sup>[a]</sup> Sanghamitra Atta,<sup>[a]</sup> N. D. Pradeep Singh,<sup>\*[a]</sup>  
Dibakar Deb,<sup>[a]</sup> W. Scott Kassel,<sup>[b]</sup> and Manish Bhattacharjee<sup>\*[a]</sup>

**Keywords:** Photodegradation / Green chemistry / Dyes/pigments / Iron / Amino acids / Biomimetic synthesis

A new biogenic potentially tetradentate ligand, L-2-(3,5-di-*tert*-butyl-2-hydroxybenzylamino)succinic acid, has been synthesized. Upon reaction with  $\text{FeCl}_3$  in the presence of triethylamine, it afforded the complex  $[\text{Et}_3\text{NH}][\text{Fe}(\text{HL})_2]$  (**1**). The complex was structurally characterized and was used for

homogeneous photocatalytic degradation of methylene blue (MB), malachite green (MG), crystal violet (CV) and rhodamine B (RhB) under visible-light irradiation in aqueous solution in the presence of  $\text{H}_2\text{O}_2$ .

## Introduction

Iron-promoted photo-Fenton systems have been used for the photodegradation of pollutants such as phenols,<sup>[1–5]</sup> chlorophenoxy herbicides<sup>[6]</sup> and different dyes<sup>[7,8]</sup> because they exhibit an accelerated rate of oxidation.<sup>[9]</sup> The two important steps that occur in photo-Fenton processes are (i) photoreduction of iron(III) to iron(II) by photoinduced metal–heteroatom bond cleavage<sup>[10]</sup> or by ligand-to-metal charge transfer<sup>[11]</sup> and (ii) reaction of  $\text{H}_2\text{O}_2$  with iron(II) to produce a reactive hydroxyl radical. Photo-Fenton processes that involve various iron complexes such as ferrioxalate/ $\text{H}_2\text{O}_2$ <sup>[12]</sup> by using UV radiation have been used for effective photodegradation of wastewater and organic pollutants. Since the major portion of sunlight falls in the visible region, utilization of visible light to degrade pollutants is highly desirable. Recently, complexes such as iron tetrasulfophthalocyanine,  $[\text{Fe}(\text{PcS})]$ , iron(II) bipyridine complex,  $[\text{Fe}(\text{bipy})_3]^{2+}$ , and iron salen complex,  $[\text{Fe}^{\text{III}}\text{-salen}]\text{Cl}$  [salen = 2,2'-ethylenebis(nitrilomethylidene)diphenol], in the presence of hydrogen peroxide have been shown to be effective catalysts for the photodegradation of organic pollutants under visible light.<sup>[13–15]</sup> It has been mentioned in the literature that  $[\text{Fe}(\text{PcS})]$  is the best choice, since it is a biomimetic catalyst and can be anchored to Amberlite. It might be

noted that, although  $[\text{Fe}(\text{Pcs})]$  is available commercially, it is not very cheap. Thus, reports on efficient photocatalysts for degradation that contain iron complexes of environmentally friendly biomimetic ligands are not numerous and the development of such complexes still remains a challenge.

Among the various organic pollutants, different synthetic dyes are widely used to colour products in many industries such as textile, paper, rubber, plastics and cosmetics. Such colouring agents, when mixed with water and used for industrial processes, produce highly coloured effluent. These common industrial pollutants are subsequently discharged mostly into surface water resources. Even at low concentrations, dyes can be detected visually and their presence in surface water affects aquatic life.<sup>[16]</sup> These highly persistent coloured compounds are not only the first visually detectable contaminant present in the water; they also inhibit the admission of sunlight into water and thus affect photosynthesis by aquatic plants.<sup>[17]</sup> Hence, it has become essential to develop a suitable process that can mineralize these kinds of contaminants present in wastewater.

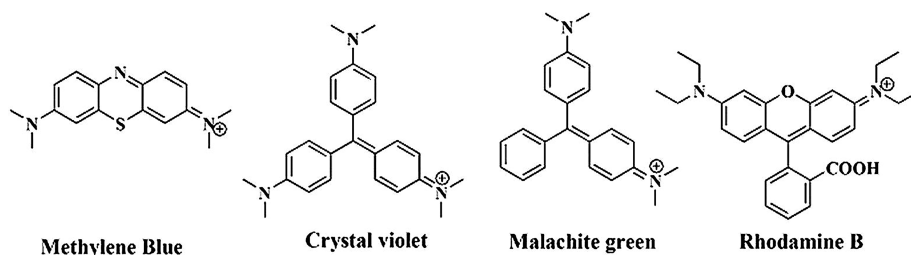
Previous studies suggest that a complex with broad absorption in the visible region can be utilized in the photo-Fenton reaction to harvest visible light. It should be noted that some of the reported complexes employ ligands that are not environmentally benign. Thus there is a need to develop iron complexes that contain environmentally friendly ligands and that show ligand-to-metal charge-transfer (LMCT) transitions in the visible region. Therefore we thought of synthesizing a ligand based on a naturally occurring amino acid that contained a phenolate group.

Herein we report the synthesis of a new amino acid based ligand, L-2-(3,5-di *tert*-butyl-2-hydroxybenzylamino)succinic acid ( $\text{LH}_3$ ), and its iron complex,  $[\text{Et}_3\text{NH}][\text{Fe}(\text{LH})_2]$

[a] Department of Chemistry, Indian Institute of Technology, Kharagpur 721302, India  
E-mail: mxb@iitkgp.ac.in;  
ndpradeep@chem.iitkgp.ernet.in  
<http://www.chemistry.iitkgp.ac.in/~mxb/>  
<http://www.chemistry.iitkgp.ac.in/faculty/NDPS/>

[b] Department of Chemistry, Villanova University, Villanova, PA 19085, USA

Supporting information for this article is available on the WWW under <http://dx.doi.org/10.1002/ejic.201402314>.



Scheme 1. Structure of cationic dyes used in the present study.

(1), as well as studies on how compound 1 catalyzed the visible-light-induced photodegradation of four cationic dyes, methylene blue (MB), malachite green (MG), crystal violet (CV) and rhodamine B (RhB), which are widely used as industrial dyes (Scheme 1).

## Results and Discussion

### Synthesis and Characterization of Ligand LH<sub>3</sub>

The sodium salt of the ligand L-2-(3,5-di-*tert*-butyl-2-hydroxybenzylamino)succinic acid was synthesized by a one-pot Mannich reaction of L-aspartic acid, formaldehyde and 2,4-di-*tert*-butyl phenol in the presence of sodium hydroxide (Scheme 2).

The ligand is soluble in methanol and ethanol and sparingly soluble in water. The diacid form was obtained by acidification of the aqueous solution of the sodium salt by dilute acetic acid; the resulting form was insoluble in water and soluble in methanol, ethanol and dimethyl sulfoxide and sparingly soluble in chloroform. The ligand was characterized by <sup>1</sup>H NMR spectroscopy, UV/Vis spectroscopy, IR and CD spectroscopy, elemental analysis and high-resolution mass spectrometry (HRMS).

The elemental analyses agree well with the proposed composition. The HRMS of NaH<sub>2</sub>L shows a molecular-ion peak at *m/z* 350.1850, which corresponds to H<sub>2</sub>L<sup>-</sup> (C<sub>19</sub>H<sub>28</sub>NO<sub>5</sub>). The isotope pattern also matches the composition. Along with this peak another peak appears at *m/z* 382.1749 (Figure S1 in the Supporting Information). This corresponds to the methanol adduct of the ligand (C<sub>20</sub>H<sub>32</sub>NO<sub>6</sub>). The isotope pattern matches the methanol adduct of the ligand. Thus the elemental analysis and the mass spectrometry support the formulation of the compound.

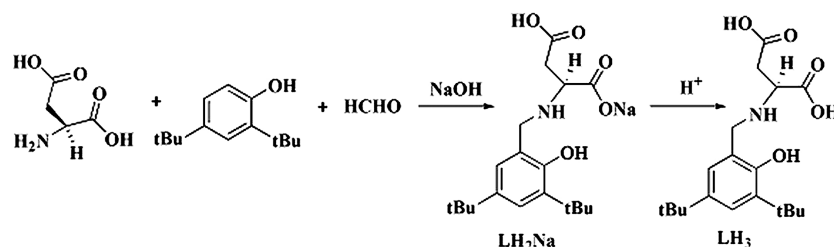
The <sup>1</sup>H NMR spectrum (CD<sub>3</sub>OD) (Figure S2 in the Supporting Information) of the LH<sub>3</sub> shows two signals at δ = 1.30 (s, 9 H) and 1.42 ppm (s, 9 H) owing to the protons of two -C(CH<sub>3</sub>)<sub>3</sub> groups. The signals for the diastereotopic methylene protons of the -CH<sub>2</sub>COOH appear at δ = 2.85 (dd, *J* = 18, 8.4 Hz, 1 H) and 3.03 ppm (dd, 4 Hz, 1 H). The signal for the -CH proton of the -NH(CH) group appears at δ = 3.95 ppm (dd, 1 H, *J* = 16, *J* = 4 Hz). The signal for the diastereotopic methylene proton of the -CH<sub>2</sub>Ph group appears at δ = 4.23 (d, 1 H, *J* = 12.8 Hz) and 4.34 ppm (d, 1 H, *J* = 13.2 Hz). The signals due to the aromatic protons appear at δ = 7.21 (d, *J* = 1.6 Hz) and 7.38 ppm (d, *J* = 1.6 Hz).

The UV/Vis spectrum of LH<sub>2</sub>Na in methanol shows two bands at 230 (ε = 2738) and 273 nm (ε = 1880) owing to the π-π\* transition (Figure S3 in the Supporting Information). The FTIR spectrum of LH<sub>2</sub>Na shows, along with other peaks, aliphatic C-H stretching at 2960 cm<sup>-1</sup> and ν<sub>as</sub>(COO) stretching at 1583 and ν<sub>s</sub>(COO) at 1480 cm<sup>-1</sup> (Figure S4 in the Supporting Information). The circular dichroism spectrum of LH<sub>2</sub>Na shows a signal with a positive Cotton effect at 220 nm and one signal with a negative Cotton effect at 254 nm owing to π-π\* transitions (Figure S5 in the Supporting Information).

### Synthesis and Characterization of Complex [Et<sub>3</sub>NH][Fe(HL)<sub>2</sub>] (1)

Ligand H<sub>3</sub>L, upon treatment with an aqueous solution of FeCl<sub>3</sub> in methanol and triethylamine in a 2:1:2 ratio, yielded the mononuclear complex 1.

The complex is soluble in common organic solvents and water. The iron complex was characterized by IR and UV/Vis spectroscopy and elemental analyses and its electrochemical properties were studied by using cyclic voltammetry.



Scheme 2. Synthesis of L-2-(3,5-di-*tert*-butyl-2-hydroxybenzylamino)succinic acid.

try and differential pulse voltammetry (DPV) and magnetic-susceptibility measurements. The elemental analyses agree well with the proposed composition. The IR spectrum of the compound along with other bands shows a broad band at  $3445\text{ cm}^{-1}$  that is due to hydrogen-bonded O–H stretching of the free carboxylate of the monomer that is involved in dimer formation (see below). The other sharp band at  $1628\text{ cm}^{-1}$  is due to the stretching of the coordinated carboxylate to metal centre. The marked shift of the carboxylate stretching from those of the ligand clearly shows that the ligand is bonded to the metal centre through the carboxylate oxygen (Figure S6 in the Supporting Information). The UV/Vis spectrum of a solution of the complex in methanol shows an absorption at  $520\text{ nm}$  ( $\epsilon = 20400$ ) along with a shoulder at  $335\text{ nm}$  ( $\epsilon = 32370$ ). These two transitions can be attributed to the phenolate-to-metal charge-transfer transitions. Along with these two bands, two strong absorptions are observed at  $290\text{ nm}$  ( $\epsilon = 36310$ ) and  $260\text{ nm}$  ( $\epsilon = 36220$ ). These bands are due to intraligand  $\pi$ – $\pi^*$  transitions (Figure S7 in the Supporting Information). The CD spectrum of the compound in methanol shows a band with a negative Cotton effect at  $210\text{ nm}$  and two bands with a positive Cotton effect at  $245$  and  $275\text{ nm}$ . A comparison with the ligand CD spectrum indicates that these signals are due to an intraligand  $\pi$ – $\pi^*$  transition. In addition to these intraligand transitions, two bands with a negative Cotton effect appear at  $290$  and  $330\text{ nm}$  and a band with a positive Cotton effect appears at  $530\text{ nm}$  (Figure S8 in the Supporting Information). These bands might be assigned to ligand-to-metal charge-transfer transitions. The electron-transfer behaviour of the complex has been studied in acetonitrile by using cyclic voltammetry. The cyclic voltammogram of the complex is not very well resolved; however, differential pulse voltammetry shows three oxidative responses at  $0.80$ ,  $0.97$  and  $1.31\text{ V}$  (Figure S9 in the Supporting Information). These oxidative responses are attributed to the following oxidation process. The first and second responses are due to the ligand-based oxidation (as both have the same ionization potential (ip) value and have a similar potential to known one-electron oxidation processes under identical conditions), which is phenoxide-to-phenoxyl-radical oxidation and can be utilized to generate mono- and bis-iron(III) phenoxyl radical. The third response might be due to  $\text{Fe}^{\text{III}} \rightarrow \text{Fe}^{\text{IV}}$  oxidation. The room-temperature magnetic moment of the compound, measured by the Gouy method, was found to be  $5.9\text{ BM}$ , which is typical of a high-spin iron(III) centre.

### Single-Crystal X-ray Structure of 1

The compound crystallizes in chiral orthorhombic space group  $P2_12_12$ . The asymmetric unit consists of an iron centre coordinated to two protonated ligands and a triethylammonium ion (Figure 1). The observed absolute structure (Flack) parameter  $[0.03(2)]^{[18]}$  clearly shows that the coordinates correspond to the absolute structure of the molecules in the crystal. The iron(III) centre is coordinated to two

nitrogen atoms, two phenoxide oxygen atoms and two carboxylate oxygen atoms from two ligands. Therefore, although the ligand is potentially tetradentate, it acts like a tridentate ligand with a pendant protonated carboxylic acid group. Two secondary nitrogen atoms (N1, N2) and two phenolate oxygen atoms (O1, O6) occupy the corners of the equatorial plane of the coordination polyhedron and the axial positions are occupied by the two carboxylate oxygen atoms, O2 and O7. Unlike tridentate Schiff base ligands,  $\text{HL}^{2-}$  in **1** adopts the facial coordination mode, presumably on account of its stereochemical flexibility. The iron centre is in a highly distorted octahedral environment as evidenced by the observed bond angles [ $\angle\text{O6–Fe1–O1} = 97.90(12)^\circ$ ,  $\angle\text{O1–Fe1–N1} = 86.62(12)^\circ$ ,  $\angle\text{N1–Fe1–N2} = 90.11(12)^\circ$ ,  $\angle\text{O2–Fe1–O7} = 157.17(13)^\circ$ ]. The bond lengths  $\text{Fe1–O2}$  [ $2.037(3)\text{ \AA}$ ] and  $\text{Fe1–O7}$  [ $2.037(3)\text{ \AA}$ ] are comparable to those observed in the iron complexes of related ligands ( $\text{Fe–O}_{\text{carboxylate}} \approx 1.95\text{–}2.09\text{ \AA}$ )<sup>[19–21]</sup> The iron phenolate oxygen bond lengths,  $\text{Fe1–O1}$  [ $1.900(3)\text{ \AA}$ ] and  $\text{Fe1–O6}$  [ $1.883(3)\text{ \AA}$ ], are similar to those reported for the six-coordinate high-spin iron(III) phenolate complexes. Typically, high-spin iron(III)–phenolate distances range from  $1.88$  to  $1.93\text{ \AA}$ .<sup>[21–24]</sup> Likewise, the iron–nitrogen bond lengths,  $\text{Fe1–N1}$  [ $2.187(4)\text{ \AA}$ ] and  $\text{Fe1–N2}$  [ $2.217(3)\text{ \AA}$ ], are comparable to those observed in similar complexes ( $\text{Fe–N}_{\text{amine}} \approx 2.16\text{–}2.38\text{ \AA}$ ) in octahedral geometry.<sup>[19,20]</sup>

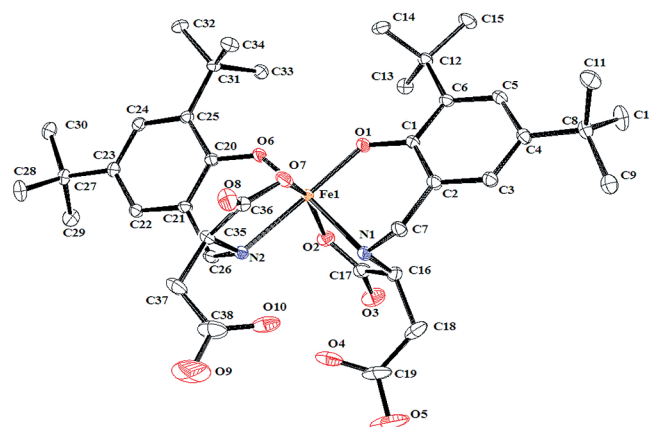


Figure 1. ORTEP view of  $[\text{FeL}_2]^+$  cation. Hydrogen atoms and  $[\text{Et}_3\text{NH}]^+$  have been omitted for clarity.

The proton on the nitrogen of  $[\text{Et}_3\text{NH}]^+$  (N3H) shows a hydrogen-bonding interaction with one of the iron-bound carboxylate oxygen atoms, (O8), [ $\text{N3}\cdots\text{O8}$   $2.814(5)\text{ \AA}$  and  $\text{H3}\cdots\text{O8}$   $1.926\text{ \AA}$ ]. Apart from this, intramolecular hydrogen bonding exists between the hydrogen atoms on the ligand nitrogen atoms, N1 and N2, and oxygen atoms, O4 and O10, of nonbonded carboxylic acid groups, respectively. In addition, intermolecular hydrogen bonding exists in the solid state between two molecules. Two molecules are hydrogen-bonded with each other through hydrogen-bonding interactions between the free  $-\text{COOH}$  groups. The hydrogen bonded to the free carboxylic acid group, H4, of one molecule is hydrogen-bonded with the  $-\text{OH}$  oxygen of  $-\text{COOH}$ , O10, of the second molecule. Similarly, the

hydrogen atom of the free  $-\text{COOH}$  group of the second molecule, H10, is hydrogen-bonded with O4 of the first molecule [H–O10 1.8200 Å; O4–O10 2.536(6) Å;  $\angle\text{O4–H4–O10}$  142.00°]. Thus two molecules form a double-helical structure through hydrogen bonding (Figure 2). It should be noted that hydrogen-bonded helical structures are not numerous in coordination compounds.

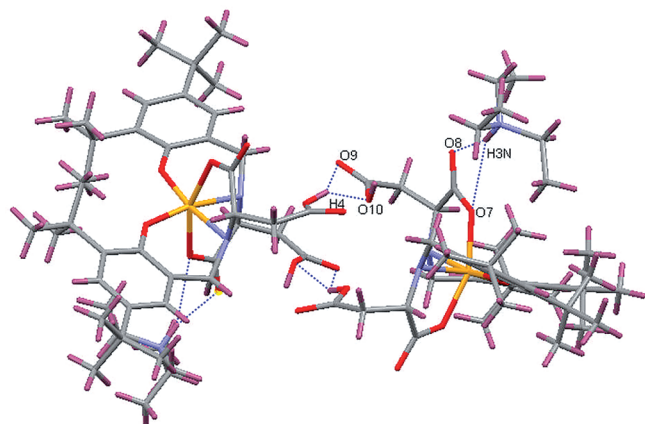


Figure 2. View of the inter- and intramolecular hydrogen bonding in **1**. Colour code: Fe, yellow; O, red; N, light blue; C, grey; H, red; hydrogen bonding, blue dotted line.

### Degradation of Methylene Blue (MB) Dye Using the Iron(III) Complex **1**

The UV/Vis spectrum of **1** shows a strong charge-transfer band in the visible region, which led us to examine the efficacy of **1** as a catalyst for the photodegradation of dyes. As a test case we first examined **1**-catalyzed degradation of methylene blue (MB). The UV/Vis spectrum of MB in water shows three absorption peaks at 246 and 291 nm and a high-intensity peak at 663 nm. The peaks at 291 and 663 nm were used for the analysis during decolorization and degradation of MB. The change in the absorption spectra of the solution was monitored by UV/Vis spectroscopy

at regular time intervals, which is shown in Figure 3 (A). The kinetics of the degradation of MB under various degradation conditions is depicted in curves 1–6 of Figure 3 (B).

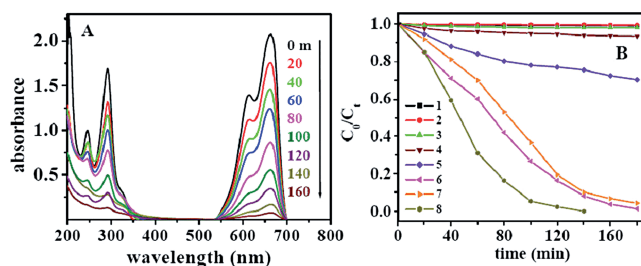


Figure 3. (A) Absorption spectra of MB dye during the degradation under visible light in the presence of **1** ( $8.5 \times 10^{-5}$  M) +  $\text{H}_2\text{O}_2$  (3 mM) at different times. (B) Degradation kinetics of MB dye ( $60 \text{ mg L}^{-1}$ ) under different conditions: (1) Only dye + light; (2) dye + **1** + light; (3) dye + **1** +  $\text{H}_2\text{O}_2$  in the dark; (4) dye +  $\text{H}_2\text{O}_2$  + light; (5) dye + **1** +  $\text{H}_2\text{O}_2$  + *i*PrOH + light; (6) dye + FePcS +  $\text{H}_2\text{O}_2$  + light; (7) dye + **1** +  $\text{H}_2\text{O}_2$  + light; and (8) dye + Fe–salen +  $\text{H}_2\text{O}_2$  + light.

When the aqueous solution of only MB and that of MB and **1** were exposed to visible light, no degradation could be observed (Figure 3, B, curves 1 and 2). Similarly, we could detect only 5% degradation of MB in the presence of **1** and  $\text{H}_2\text{O}_2$  in the dark (Figure 3, B, curve 3). When an aqueous solution of MB and  $\text{H}_2\text{O}_2$  was irradiated with visible light, a very small amount (10%) of degradation was observed (Figure 3, B, curve 4). However, when an aqueous solution of MB, **1** and  $\text{H}_2\text{O}_2$  was irradiated with visible light, the degradation was found to be efficient (Figure 3, B, curve 7, 90% after 4 h) and displayed first-order reaction kinetics with a rate constant of  $k = 5.36 \times 10^{-4} \text{ s}^{-1}$  (Figure 4).

Hence the experimental results suggest that the iron catalyst and  $\text{H}_2\text{O}_2$  are necessary ingredients for the degradation reaction under visible-light irradiation. Again, to verify the formation of reactive oxygen species, hydroxyl radicals, in this photo-Fenton process, the degradation reaction was studied in the presence of a well-known hydroxyl radical scavenger, 2-propanol, under visible-light conditions. It was found that in the presence of 2-propanol, degradation of MB was lower (35%, 4 h, Figure 3, B, curve 5). This experimental result indicates that hydroxyl radical generated in

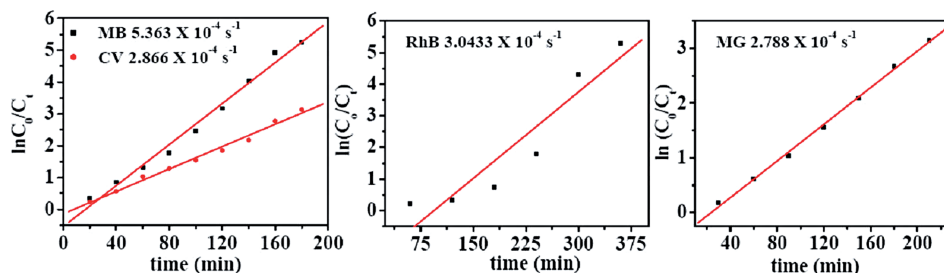


Figure 4. Degradation kinetics [ $\ln(C_0/C_t)$  versus time] of MB, CV, RhB and MG dye.

the reaction medium is the key species responsible for the degradation.

We have compared the degradation efficiency of **1** with that of two reported iron complexes, [Fe(PcS)] and [Fe<sup>III</sup>-salen] (Figure 3, B, curve 6 and 8, respectively) and the efficiency of **1** was found to be comparable to that of [Fe(PcS)] and [Fe<sup>III</sup>-salen].

### Effect of Hydrogen Peroxide on Degradation

In the Fenton system, concentration of H<sub>2</sub>O<sub>2</sub> has an important role in the generation of hydroxyl radicals. To find out the optimum concentration of H<sub>2</sub>O<sub>2</sub> required, the newly prepared iron complex (8.5 × 10<sup>-5</sup> M) was used in the photodegradation of MB (1.87 × 10<sup>-4</sup> M) under visible light in the presence of different amounts of H<sub>2</sub>O<sub>2</sub> (1–8 mM). It has been observed that with an increase in the concentration of H<sub>2</sub>O<sub>2</sub>, the rate of degradation of MB increases. The maximum degradation (90%, 4 h) has been observed at a 3 mM concentration of H<sub>2</sub>O<sub>2</sub>, and with a further increase in the concentration, the rate of the degradation decreases (Figure 5). This is because of the fact that in the presence of a low concentration of H<sub>2</sub>O<sub>2</sub>, the formation of the ·OH radical is lower, thus leading to the inefficient degradation. Similarly, when a high concentration of H<sub>2</sub>O<sub>2</sub> is used, the ·OH radicals produced react with the excess amounts of H<sub>2</sub>O<sub>2</sub> to produce ·OOH radical and H<sub>2</sub>O, and consequently, the rate of degradation decreases.<sup>[25]</sup> Thus the optimum concentration of H<sub>2</sub>O<sub>2</sub> was found to be 3 mM for the degradation of MB (1.87 × 10<sup>-4</sup> M).

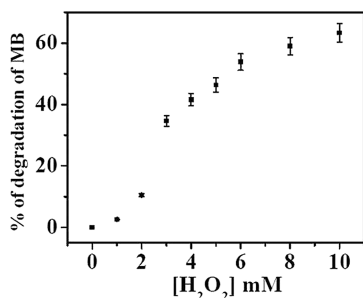


Figure 5. Effect of different concentrations of hydrogen peroxide on the degradation of MB after 2 h.

### Effect of the Concentration of the Iron Complex on Degradation

Since both iron(II/III) and H<sub>2</sub>O<sub>2</sub> are responsible for the production of the highly oxidizing species, hydroxyl radical, in any Fenton or photo-Fenton system, in addition to the concentration of H<sub>2</sub>O<sub>2</sub>, the concentration of iron species is also important. Therefore, to determine the optimum concentration of the catalyst, the photodegradation of MB (1.87 × 10<sup>-4</sup> M) was carried out, by varying the concentration of **1** (0–9 × 10<sup>-5</sup> M) in the presence of H<sub>2</sub>O<sub>2</sub> (3 mM) (Figure 6, A). From the experimental results it was observed that after a long period of irradiation, the percentage degradation of MB was very low (only 10%, 4 h) in the

absence of **1**. But, as expected, with an increase in the concentration of **1**, the percentage of degradation was found to increase and reached a maximum value at a concentration of 8.5 × 10<sup>-5</sup> M (complete degradation: 4 h). With a further increase in the concentration of the catalyst, the percentage of degradation of MB remained almost unchanged. Thus for subsequent photodegradation experiments 8.5 × 10<sup>-5</sup> M catalyst was used as the optimum catalyst concentration. Furthermore, to understand the effect of H<sub>2</sub>O<sub>2</sub> and light, the iron complex (without dye) was irradiated in the presence of H<sub>2</sub>O<sub>2</sub> under visible light. The irradiated complex solution was analyzed by UV/Vis spectroscopy (Figure 6, B), which shows a gradual decrease in the absorbance at 500 nm and gradual increase in the absorbance in the 400 nm region, which indicates the formation of iron-coordinated phenoxyl radical species.<sup>[26]</sup>

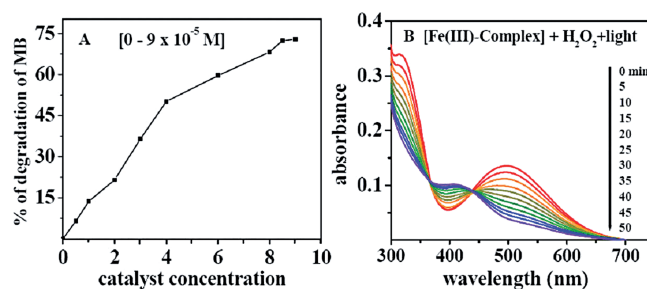


Figure 6. (A) Effect of different concentration of iron catalyst on the degradation of MB. (B) Change in iron complex alone by H<sub>2</sub>O<sub>2</sub> in the presence of light.

After visible-light irradiation of the complex for 30 min in the presence of H<sub>2</sub>O<sub>2</sub>, the solution was treated with concentrated hydrochloric acid, the ligand was extracted with chloroform and upon evaporation the chloroform solution afforded a white solid. The <sup>1</sup>H NMR spectrum of the solid was recorded and the spectrum was found to be exactly the same as that of the ligand. Thus it is clear that there is no degradation of the ligand. Also, it has been shown that this kind of ligand produces stable metal-coordinated phenoxyl radical.<sup>[26]</sup>

### Effect of pH on Degradation

It has been shown that the pH of the solution also has an important role in degradation.<sup>[27,28]</sup> To determine the effect of pH on the degradation reaction, first the stability of the iron complex was determined under different pH conditions. It was found that the newly prepared iron complex is stable in the pH range of 3–10. Therefore photodegradation of MB was examined in the pH range of 3.12 to 9.88 (Figure 7).

In all experiments, the pH of the solution was adjusted by adding an appropriate amount of NaOH or HCl solution. It was observed that with an increase in pH, from 7.0 to 9.82, the percentage of degradation also increases. This is probably because of the fact that in an alkaline medium the iron complex becomes a negatively charged species and as the dye MB is cationic in nature, there is an electrostatic

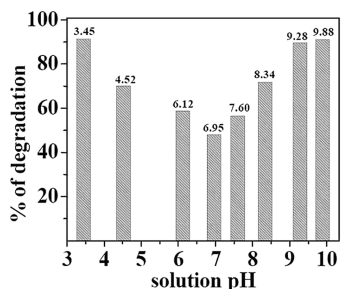


Figure 7. Effect of pH of medium on the degradation of MB.

interaction between the catalyst and MB that facilitates them coming in close proximity.<sup>[29]</sup> The degradation rate of MB was also investigated at pH 6.12, and at this pH it was observed that the degradation rate was higher than that under the neutral (pH  $\approx$  7) conditions. The percentages of degradations were found to be 85.2, 90.4, 84.9 and 76.6% at pH 3.45, 9.88, 6.12 and 7.12, respectively, after 2 h of irradiation. It can be seen that the rate of degradation increases with a decrease in pH from 6.95 to 3.45. This is due to the fact that generation of Fe<sup>II</sup> increases with the decrease in pH. Thus it can be concluded that at constant time, the percentage of degradation varies with the pH of the solution.<sup>[30]</sup>

### Effect of Salts on Degradation

In the textile industry, various types of auxiliaries are employed with dye materials in colourization processes. Therefore textile waste streams contain elevated levels of other salts and ions in addition to dyes.<sup>[31]</sup> To evaluate the individual effect of added salts in the decolorization and degradation of dyes, photodegradation of MB by **1** was carried out in the presence (0.01 M) of sodium salts of chloride, nitrite, nitrate and carbonate ions while maintaining all other experimental conditions fixed as before.

The effect of different added ions in the degradation of MB is shown in Figure 8. It has been observed that, in the absence of any salt, MB degrades 90.4% after 2 h of irradiation but in the presence of sodium salts of chloride and nitrite the percentage of degradation decreases. Similar observations were also made in some recent studies.<sup>[32–34]</sup> Generally, anions such as chloride and nitrite react with the reactive oxygen species, hydroxyl radicals. This results in

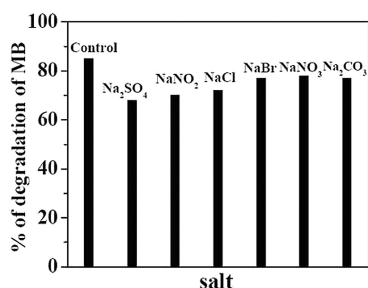


Figure 8. Effect of different salts on the degradation of MB after 3 h of irradiation.

less availability of the hydroxyl radicals in the reaction medium. The degradation rate of MB has also been found to decrease in the presence of sodium carbonate because it acts like a free-radical scavenger.<sup>[30]</sup>

### Detection of Active Oxidant Species

In any photo-oxidative degradation reaction, the detection of reactive oxygen species involved is very important as it helps to understand the degradation mechanism and the pathways. Hence, to search for the reactive oxygen species produced in the present degradation study, a series of reactions was conducted by using different selective scavengers. Some specific agents such as 2-propanol (2-propanol/H<sub>2</sub>O = 1:20), methanol (CH<sub>3</sub>OH/H<sub>2</sub>O = 1:4) and benzoquinone (BQ;  $c = 1 \text{ mmol L}^{-1}$ ) were added to the reaction solution separately to detect the active species in the degradation process. No significant change in the degradation rate was observed when BQ (O<sub>2</sub><sup>-</sup> quencher) was added into the reaction medium. Thus involvement of superoxide radical anions (O<sub>2</sub><sup>-</sup>) can be ruled out. However, in the presence of 2-propanol, a hydroxyl radical scavenger, the rate of degradation was found to decrease drastically (only 35% degradation of MB occurred over 4 h). This indicates that hydroxyl radicals are the key active oxidant that is responsible for the degradation. The same thing was observed when another hydroxyl radical scavenger, methanol, was used. For a better understanding, we carried out spin-trapping EPR experiments using 5,5-dimethyl-1-pyrroline *N*-oxide (DMPO) as a spin trap. Unfortunately, no characteristic peaks of the DMPO–OH adduct were detected. Similar results are also reported in the literature.<sup>[35]</sup>

Furthermore, to confirm the formation of hydroxyl radicals in the present system, the detection of  $\cdot\text{OH}$  radicals was carried out by means of the benzoic acid hydroxylation method.<sup>[36]</sup> Benzoic acid is known to react with hydroxyl radical and form salicylic acid, which reacts with iron(III) to produce a violet-coloured salicylatoiron(III) complex that shows an intense band at 520 nm. Thus, benzoic acid was added to a Pyrex tube. Hydrogen peroxide and **1** were added to this and the reaction solution was irradiated with visible light. At intervals of 20 minutes the solution was analyzed by means of UV/Vis spectroscopy (Figure 9). The

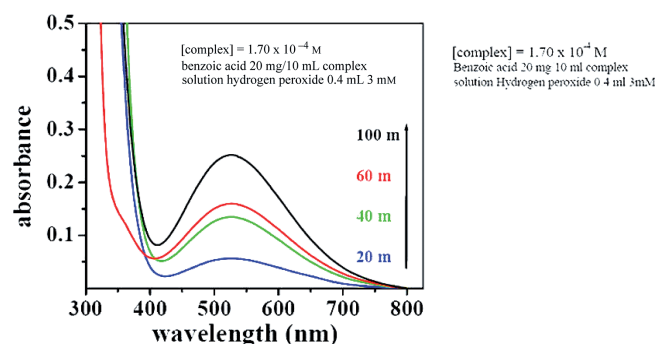


Figure 9. Absorption spectra of tetraaqua-salicylatoiron(III) complex generated by complexation of iron(III) by salicylic acid at different irradiation times.

spectrum shows a characteristic peak of the salicylate complex of iron at  $\lambda_{\text{max}} = 520 \text{ nm}$ .<sup>[35]</sup> It was found that the intensity of the peak increases with an increase in irradiation time of photolysis (Figure 9). Thus it is clear that the hydroxyl radical produced reacts with benzoic acid to afford salicylic acid, which forms a complex with iron(III).

### Probable Degradation Mechanism

The control experiments clearly indicate that the hydroxyl radical is the oxidizing agent in the **1**-catalyzed photodegradation of MB by hydrogen peroxide. To gain insight into the reaction, we carried out experiments to establish the generation of iron(II) in the reaction. Thus, the aqueous solution of **1** ( $8.50 \times 10^{-5} \text{ M}$ ) in the presence of 3 mM of  $\text{H}_2\text{O}_2$  was irradiated under visible light. After a certain interval of time, a measured (2 mL) amount of aliquot was taken and mixed with an aqueous solution of **1** (2 mL) and 10-phenanthroline and the mixture was preserved in the dark for 1 h. Then UV/Vis spectra of the solutions were recorded. The concentration of  $\text{Fe}^{\text{II}}$  ions was determined from the absorbance at 510 nm.<sup>[37]</sup> The experimental results reveal that under visible-light irradiation the iron(III) complex can produce an iron(II) complex in the presence of  $\text{H}_2\text{O}_2$ .

In the literature it has been shown that dyes can absorb visible light and become excited into a higher-energy state from which they can transfer an electron to iron(III) to produce iron(II) species. However, it is clear from the experimental results that in this case iron(II) is produced from the iron(III) complex in the reaction medium in the presence of light. The iron(II) complex produced reacts with  $\text{H}_2\text{O}_2$  and generates hydroxyl radicals by means of a classical Fenton reaction. These hydroxyl radicals are responsible for the degradation of organic dyes.

On the basis of the degraded products of MB and the information from previous reports, a probable mechanistic pathway of degradation has been proposed that is shown in Scheme 3. We suggest that the iron(III) complex **1** under visible-light irradiation undergoes internal electron transfer to produce an iron(II)-coordinated phenoxyl radical and the iron(II) complex produced in the reaction medium re-

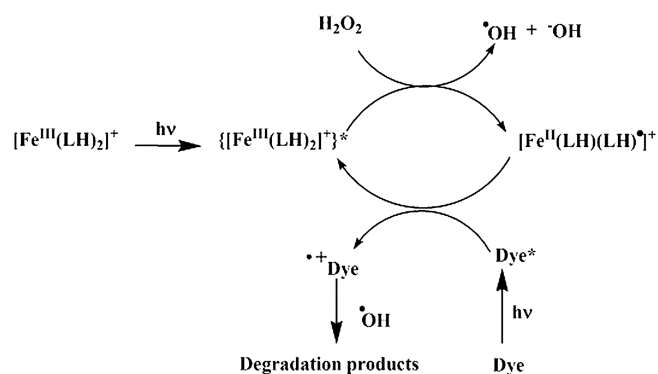
acts with hydrogen peroxide to produce the hydroxyl radical that is responsible for MB degradation. A similar kind of mechanism has been predicted in the 5-sulfosalicylic acid complex of iron(III).<sup>[38]</sup>

### The FTIR Analysis of the Intermediates During the Photodegradation of MB

To study the degradation mechanism of the dyes, the intermediates produced during the photodegradation reaction of MB at different reaction times were examined by means of infrared spectroscopy (Figure S10 in the Supporting Information). In this experiment, a high-concentration aqueous solution of MB was chosen for degradation to observe the clear change during degradation. The FTIR spectrum of pure MB shows characteristic bands of the C=N ring stretch at  $1600 \text{ cm}^{-1}$ , C=C at  $1491 \text{ cm}^{-1}$ , the symmetric C-N stretch at  $1395 \text{ cm}^{-1}$  and the N-CH<sub>3</sub> accompanied with CH<sub>3</sub> bending vibrations at 2815, 2861 and  $2949 \text{ cm}^{-1}$ . The band for the C-S stretch appears in the  $700\text{--}570 \text{ cm}^{-1}$  region.<sup>[39,40]</sup> The band at 2861 and  $2815 \text{ cm}^{-1}$  gradually decreases with an increase in irradiation time. This phenomenon has also been found in earlier reports to indicate demethylation of the -N(CH<sub>3</sub>)<sub>2</sub> group that is present in MB dye. During degradation, a broad band in the range of  $3500\text{--}3400 \text{ cm}^{-1}$  was observed, which might be due to the formation of various functional groups such as -NH<sub>2</sub>, -COOH and -OH. The FTIR spectrum after 4 h of irradiation (required for complete decolourization) shows the disappearance of the characteristic peaks at  $1600 \text{ cm}^{-1}$  (for C=N), at  $1491 \text{ cm}^{-1}$  (for C=C) and peaks in the range of  $700\text{--}570 \text{ cm}^{-1}$  (responsible for the C-S bond). A new peak appears at  $1648 \text{ cm}^{-1}$  that might be due to the formation of an amide group or R-NH<sub>3</sub><sup>+</sup>.<sup>[38,40]</sup> The results obtained from the FTIR study indicate that the cleavage of the core ring structure of the MB dye occurs along with demethylation.

### Probable Degradation Products of Methylene Blue

To identify the degradation end products, liquid chromatography-mass spectrometry (LC-MS) analysis was carried out after the complete photodegradation reaction of MB solution. Identification of all compounds present in the solution could not be carried out. The LC-MS spectrum (Figure S11 in the Supporting Information) shows an intense peak at  $m/z$  123 owing to the formation of *N*-methylaniline as a major product. The peak at  $m/z$  108 revealed the presence of another degraded product, 1,4-diaminobenzene. Other small peaks at  $m/z$  73, 85 and 100 showed that newly prepared iron(III) complex **1** can efficiently degrade the organic dye MB.<sup>[30,41]</sup> On the basis of the degradation products (identified by LC-MS) it has been found that the MB dye undergoes successive demethylation followed by aromatic ring cleavage during the degradation process.



Scheme 3. Proposed mechanism for the degradation of dye by complex **1** under visible light.

## Degradation of Other Dyes Such as Crystal Violet (CV), Malachite Green (MG) and Rhodamine B (RhB) by Using 1

To further prove the versatility of the complex in photodegradation, the degradation of CV, MG and RhB dyes was carried out in the presence of **1**. A  $1.42 \times 10^{-4}$  M solution of CV was used for photodegradation under same reaction conditions as described above for the degradation of MB. The UV/Vis spectrum of CV shows a peak at 585 nm. The change in the absorption spectra of CV during photocatalytic degradation is shown in Figure 10 (A). The kinetic study under different conditions is represented in curves 1–6 of Figure 10 (B). On the basis of the results it was found that the complete decolourization of CV took place in 3.5 hours under the optimum conditions.

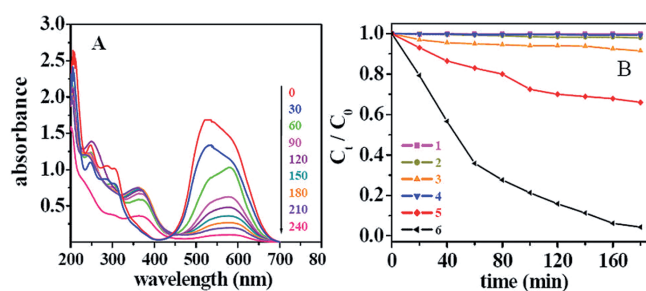


Figure 10. (A) Absorption spectra of CV during the degradation under visible light in the presence of **1** with  $\text{H}_2\text{O}_2$  at different times. (B) Degradation CV under different conditions: (1) Dye + light; (2) dye + **1** + light; (3) dye + **1** +  $\text{H}_2\text{O}_2$ ; (4) dye +  $\text{H}_2\text{O}_2$  + light; (5) dye + **1** +  $\text{H}_2\text{O}_2$  + *i*PrOH + light; and (6) dye + **1** +  $\text{H}_2\text{O}_2$  + light.

Similarly, MG ( $6.50 \times 10^{-4}$  M,  $\lambda_{\text{max}} = 618$  nm) (Figure 11) and RhB ( $2.83 \times 10^{-4}$  M and  $\lambda_{\text{max}} = 554$  nm) (Figure 12) dyes were degraded under the same conditions as those described above for the degradation of MB. It has been observed that 4 and 6 hours are required for the complete degradation of MG and RhB, respectively. The pseudo-first-order rate constants for the degradation of MG, CV and RhB were found to be  $2.79$ ,  $2.87$  and  $3.04 \times 10^{-4} \text{ s}^{-1}$ , respectively (Figure 4).

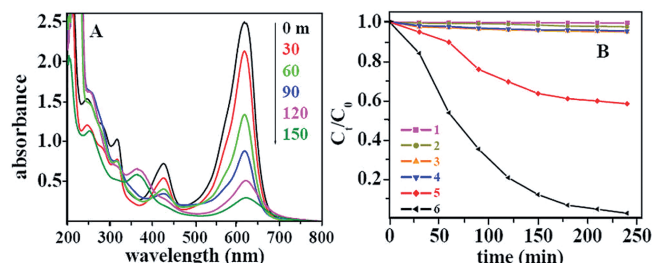


Figure 11. (A) Absorption spectra of MG during the degradation under visible light in the presence of **1** with  $\text{H}_2\text{O}_2$  at different times. (B) Degradation MG under different conditions: (1) Dye + light; (2) dye + **1** + light; (3) dye + **1** +  $\text{H}_2\text{O}_2$ ; (4) dye +  $\text{H}_2\text{O}_2$  + light; (5) dye + **1** +  $\text{H}_2\text{O}_2$  + *i*PrOH + light; and (6) dye + **1** +  $\text{H}_2\text{O}_2$  + light.

The extent of mineralization in terms of total organic carbon (TOC) for the degradation of dyes (aqueous solution) was measured by WinTOC. During this experiment,

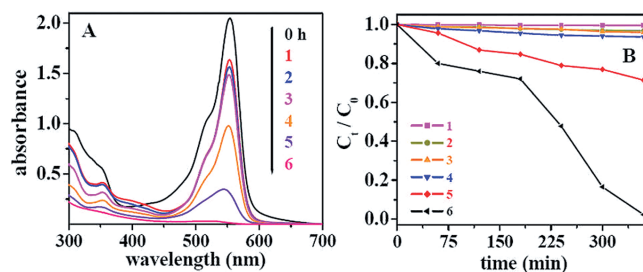


Figure 12. (A) Absorption spectra of RhB during the degradation under visible light in the presence of **1** with  $\text{H}_2\text{O}_2$  at different times. (B) Degradation RhB under different conditions: (1) Dye + light; (2) dye + **1** + light; (3) dye + **1** +  $\text{H}_2\text{O}_2$ ; (4) dye +  $\text{H}_2\text{O}_2$  + light; (5) dye + **1** +  $\text{H}_2\text{O}_2$  + *i*PrOH + light; and (6) dye + **1** +  $\text{H}_2\text{O}_2$  + light.

the TOC of the initial solution (dye/catalyst/ $\text{H}_2\text{O}_2$ ) and degraded solution were measured before and after photodegradation. Then the percentage of mineralization was obtained for different dye solutions from the difference of initial and final TOC values. From this result it was observed that TOC values dropped by 31.5, 43.5, 46.7 and 87% for MB, MG, CV and RhB, respectively, after complete decolourization. The result shows that this iron complex mediated visible-light photo-Fenton degradation provided a significant demineralization of synthetic organic dyes.

## Conclusion

In summary, we have synthesized a new amino acid based ligand and its iron(III) complex, which has been structurally characterized. This complex has been shown to be an efficient photocatalyst for the degradation of dyes such as MB, CV, MG and RhB under visible-light irradiation. Complete degradation and decolourization took place within 3–6 hours for different dyes. The optimal catalyst concentration for degradation was found to be  $8.5 \times 10^{-5}$  M and the optimal pH was 6.5.

## Experimental Section

**General:** Chemicals used were reagent-grade products. Elemental analyses were performed with a Perkin–Elmer model 2400 C, H, N analyzer.  $^1\text{H}$  and  $^{13}\text{C}$  NMR spectra were recorded in  $\text{D}_2\text{O}$  with a Bruker Avance II instrument. The IR spectra were recorded with a Perkin–Elmer model 883 spectrometer. UV/Vis spectra were recorded in solution with a Shimadzu model UV-1601 spectrophotometer. EPR spectra were recorded with a Bruker model ESP 300E spectrometer. LC–MS measurements were carried out with an Agilent 1100 series spectrometer equipped with VWD and DAD detectors and with a C8 column in a variable-temperature range of 30–280 °C. TOC values for the degradation of dyes (aqueous solution) were measured by WinTOC, using an OI Analytical Solids TOC Analyzer (model 1030) with attached autosampler (model 1088).

**Synthesis of  $\text{H}_3\text{L}$ :** L-Aspartic acid (1.33 g, 10 mmol) was dissolved in water (30 mL) that contained NaOH (0.8 g, 20 mmol). This was added to solution of 2,4-di-*tert*-butylphenol in ethanol (2.06 g, 10 mmol in 30 mL of ethanol). Aqueous formaldehyde (8 mL;

40%) was added to it. The resulting mixture was heated to reflux for 6 h at 90 °C and was kept for slow evaporation, which gave a milky white slurry. Treatment of the slurry with a large excess amount of acetone resulted in a white precipitate, which was filtered and washed by aqueous ethanol and finally hexane (to remove unreacted phenol) to obtain the sodium salt of the ligand. The acid form of the ligand, H<sub>3</sub>L, was obtained by acidification of the aqueous solution of NaHL by dilute CH<sub>3</sub>COOH. Finally the product was recrystallized from a mixture of ethanol and water (4:1); yield 82% (0.288 g). C<sub>19</sub>H<sub>28</sub>NNaO<sub>5</sub>: calcd. C 61.11, H 7.56, N 3.75; found C 61.06, H 7.49, N 3.67.

**Synthesis of [Et<sub>3</sub>NH][Fe(LH)<sub>2</sub>] (1):** Ligand LH<sub>3</sub> (0.351 g, 1 mmol) was dissolved in a mixture of methanol (20 mL) and water (5 mL) in a beaker. A solution of anhydrous FeCl<sub>3</sub> (0.08 g, 0.5 mmol) in methanol and triethylamine (0.101 g; 1 mmol, 0.14 mL) was added. The resulting blue-violet solution was stirred for an hour and then kept for slow evaporation at room temperature. Upon standing for about a week the solution gave the product, which was washed with water and then redissolved in acetonitrile, from which red-violet single crystals suitable for X-ray diffraction were obtained; yield 0.25 g; 58.2%. C<sub>44</sub>H<sub>68</sub>FeN<sub>3</sub>O<sub>10</sub> (854.86): calcd. C 61.82, H 8.02, N 4.92; found C 61.76, H 7.92, N 4.86.

**Crystal Structure Determination:** Crystal data for **1** was collected at 100 K with a Bruker Smart CCD APEX diffractometer with Mo-K<sub>α</sub> (λ = 0.71073 Å) radiation using a cold nitrogen stream. The crystal structure was solved by direct methods and refined with full-matrix least-squares cycles using SHELXL<sup>[42]</sup> with atomic coordinates and anisotropic thermal parameters for all non-hydrogen atoms.

**Crystal Data:** Empirical formula C<sub>44</sub>H<sub>68</sub>N<sub>3</sub>O<sub>10</sub>Fe; M<sub>r</sub> = 854.86, T = 100 K, λ = 0.71073 Å, crystal system: orthorhombic, space group: P2<sub>1</sub>2<sub>1</sub>2<sub>1</sub>; a = 38.6516(10) Å, b = 10.8735(3) Å, c = 12.8940(3) Å; V = 5419.1(2) Å<sup>3</sup>, Z = 4, D<sub>calcd.</sub> = 1.048, μ = 0.326, F(000) = 1836. Final R indices [I > 2σ(I)]: R = 0.0620, wR2 = 0.2758, Flack parameter: 0.03(2). Important bond lengths and bond angles are given in the Supporting Information.

CCDC-989307 contains the supplementary crystallographic data for compound **1**. These data can be obtained free of charge from The Cambridge Crystallographic Data Centre via www.ccdc.cam.ac.uk/data\_request/cif.

**Degradation Experiments:** In a 100 mL round-bottomed Pyrex flask, an aqueous solution (50 mL) that contained dye, iron catalyst and other required elements was mixed and stirred for 5 min in the dark. The solution was placed 10 cm away from the visible-light source, which was a 125 W Hg lamp with a water circulation jacket to cool the lamp. Another Pyrex jacket that contained the aqueous NaNO<sub>2</sub> solution (10% w/w) as a light filter through which only visible light (λ > 400 nm) could pass.<sup>[43]</sup>

The incident light intensity (I<sub>0</sub>) of the light source is 4.117 × 10<sup>16</sup> Einstein L<sup>-1</sup> s<sup>-1</sup>. An aqueous solution of the MB dye (1.87 × 10<sup>-4</sup> M) was subjected to degradation under different conditions. Other dyes used for degradation were RhB (1.24 × 10<sup>-4</sup> M), CV (1.47 × 10<sup>-4</sup> M) and MG (1.64 × 10<sup>-4</sup> M). The concentration of the newly prepared iron(III) complex (**1**) used for degradation was 8.50 × 10<sup>-5</sup> M in water; 3 mM hydrogen peroxide solution was used. At regular intervals of 30 min, samples (3 mL) were withdrawn from the reaction mixture solution and the concentration was measured by means of UV/Vis spectroscopy. The effects of H<sub>2</sub>O<sub>2</sub> and different salts (0.01 M each) as well as the effect of pH of the medium on the degradation of MB were investigated. After completion of the degradation reaction, LC-MS analysis was carried out

to identify the degraded products. Generation of hydroxyl radical was determined by means of the benzoic acid hydroxylation method.<sup>[44]</sup> In this method, Fe<sup>III</sup>-salicylic acid complex [tetraaquo-salicylatoiron(III) complex, λ<sub>max</sub> = 522 nm] was formed and identified by means of UV/Vis spectroscopy.

**LC-MS Analysis of MB Degradation:** The sample was prepared as follows. The mixture of MB dye solution was irradiated with visible light. When the solution was completely decolourized, the degradation products were extracted several times with ethyl acetate. The ethyl acetate extract was evaporated to dryness with a rotary evaporator. The dry residue obtained was dissolved in methanol and analyzed by LC-MS analysis.

**Supporting Information** (see footnote on the first page of this article): Spectra, electrochemical data and tables with important bond lengths and bond angles.

## Acknowledgments

The authors thank the Department of Science and Technology (DST), Government of India, New Delhi for use of its NMR spectroscopic and single-crystal X-ray facility.

- [1] V. Kavita, K. Palanivelu, *Chemosphere* **2004**, *55*, 1235–1243.
- [2] J. Kiwi, C. Pulgarin, P. Peringer, *Appl. Catal. B* **1994**, *3*, 335–350.
- [3] R. Chen, J. J. Pignatello, *Environ. Sci. Technol.* **1997**, *31*, 2399–2406.
- [4] V. Nadtochenko, J. Kiwi, *J. Photochem. Photobiol. A: Chem.* **1996**, *99*, 145–153.
- [5] P. Maletzky, R. Bauer, *Chemosphere* **1998**, *37*, 899–909.
- [6] J. J. Pignatello, *Environ. Sci. Technol.* **1992**, *26*, 944–951.
- [7] a) V. Nadochenko, J. Kiwi, *J. Chem. Soc. Faraday Trans.* **1997**, *93*, 2373–2378; b) Z. Xiong, L. L. Zhang, J. Ma, X. S. Zhao, *Chem. Commun.* **2010**, *46*, 6099–6101; c) J. M. Monteagudo, A. Durán, L. S. Martín, M. Aguirre, *Appl. Catal. B* **2010**, *96*, 486–95.
- [8] a) Y. Xie, F. Chen, J. He, J. Zhao, H. Wang, *J. Photochem. Photobiol. A: Chem.* **2000**, *136*, 235–240; b) S. Q. Liu, L. R. Feng, N. Xu, Z. G. Chen, X. M. Wang, *Chem. Eng. J.* **2012**, *203*, 432–439.
- [9] T. H. Wang, S. F. Kang, Y. H. Lin, *J. Environ. Sci. Health Part A* **1999**, *34*, 1267–1281.
- [10] K. Lang, S. Lunak, *Photochem. Photobiol. Sci.* **2002**, *1*, 588–591.
- [11] H. Kunkely, A. Vogler, *Inorg. Chem. Commun.* **2003**, *6*, 1335–1337.
- [12] a) K. A. Hislop, J. R. Bolton, *Environ. Sci. Technol.* **1999**, *33*, 3119–3126; b) J. M. Monteagudo, A. Durán, M. Aguirre, L. S. Martí'n, *J. Hazard. Mater.* **2011**, *185*, 131–139.
- [13] X. Tao, W. Ma, T. Zhang, J. Zhao, *Angew. Chem. Int. Ed.* **2001**, *40*, 3014–3016; *Angew. Chem.* **2001**, *113*, 3103.
- [14] M. Cheng, W. Ma, C. Chen, J. Yao, J. Zhao, *Appl. Catal. B* **2006**, *65*, 217–226.
- [15] S. Gazi, R. Ananthakrishnan, N. D. P. Singh, *J. Hazard. Mater.* **2010**, *1*, 588–591.
- [16] T. Robinson, G. McMullan, R. Marchant, P. Nigam, *Bioresour. Technol.* **2004**, *77*, 247–255.
- [17] I. M. Banat, P. Nigam, D. Singh, R. Marchant, *Bioresour. Technol.* **1996**, *58*, 217–227.
- [18] H. D. Flack, *Acta Crystallogr. Sect. A* **1983**, *39*, 876–881.
- [19] W. Schmitt, M. Murugesu, J. C. Goodwin, J. P. Hill, A. Mandel, R. Bhalla, C. E. Anson, S. L. Heath, A. K. Powell, *Polyhedron* **2001**, *20*, 1687–1697.
- [20] W. Schmitt, J. P. Hill, M. P. Juanico, A. Caneschi, F. Costantino, C. E. Anson, A. K. Powell, *Angew. Chem. Int. Ed.* **2005**, *44*, 4187–4192; *Angew. Chem.* **2005**, *117*, 4259.

- [21] M. S. Shongwe, C. H. Kaschula, M. S. Adsetts, E. W. Ainscough, A. M. Brodie, M. J. Morris, *Inorg. Chem.* **2005**, *44*, 3070–3079.
- [22] R. Hernandez-Molina, A. Mederos, S. Dominguez, P. Gili, C. Ruiz-Perez, A. Castineiras, X. Solans, F. Lloret, J. A. Real, *Inorg. Chem.* **1998**, *37*, 5102–5108.
- [23] M. R. McDevitt, A. W. Addison, E. Sinn, L. K. Thompson, *Inorg. Chem.* **1990**, *29*, 3425–3433.
- [24] Y. Nishida, K. Kino, S. Kida, *J. Chem. Soc., Dalton Trans.* **1987**, 1157–1161.
- [25] A. S. Stasinakis, *Global NEST J.* **2008**, *10*, 376–385.
- [26] a) L. K. Nairn, S. J. Archibald, R. Bhalla, B. C. Gilbert, E. J. MacLean, S. J. Teat, H. Walton, *Dalton Trans.* **2006**, 172–176; b) E. Bill, J. Müller, T. Weyhermüller, K. Weighardt, *Inorg. Chem.* **1999**, *38*, 5795–5802; c) P. Chaudhuri, M. Hess, J. Müller, K. Hildenbrand, E. Bill, T. Weyhermüller, K. Weighardt, *J. Am. Chem. Soc.* **1999**, *121*, 9599–9610.
- [27] Y. Wang, *Water Res.* **2000**, *34*, 990–994.
- [28] H. YingPing, L. XiangLing, F. YanFen, W. Qi, L. KingTong, *Wuhan Univ. J. Nat. Sci.* **2009**, *14*, 262–266.
- [29] R. J. Tayade, T. S. Natarajan, H. C. Bajaj, *Ind. Eng. Chem. Res.* **2009**, *48*, 10262–10267.
- [30] F. Huang, L. Chen, H. Wang, Z. Yan, *Chem. Eng. J.* **2010**, *162*, 250–256.
- [31] M. Bhati, G. Singh, *Bioresour. Technol.* **2003**, *88*, 221–228.
- [32] P. K. Malik, S. K. Saha, *Sep. Purif. Technol.* **2003**, *31*, 241–250.
- [33] F. A. Alshamsi, A. S. Albadwawi, M. M. Alnuaimi, M. A. Rauf, S. S. Ashraf, *Dyes Pigm.* **2007**, *74*, 283–287.
- [34] G. Jin-Zhang, M. Dong-Ping, C. Xiao, L. Yan, Y. Wu, *Chin. J. Appl. Chem.* **2007**, *24*, 534–539.
- [35] Z. Wang, Z. Liu, R. Cai, *Environ. Sci. Technol.* **2008**, *42*, 5759–5764.
- [36] A. Y. Satoh, J. E. Trosko, S. J. Masten, *Environ. Sci. Technol.* **2007**, *41*, 2881–2887.
- [37] A. E. Harvey Jr., J. A. Smart, E. D. Amis, *Anal. Chem.* **1955**, *27*, 26–29.
- [38] H. Ji, W. Song, C. Chen, H. Yuan, W. Ma, J. J. Zhao, *Environ. Sci. Technol.* **2007**, *41*, 5103–5107.
- [39] Z. Yu, S. C. Chuang, *J. Phys. Chem. C* **2007**, *111*, 13813–13820.
- [40] O. V. Ovchinnikov, S. V. Chernykh, M. S. Smirnov, D. V. Alpatova, R. P. Vorobeva, A. N. Latyshev, A. B. Evlev, A. N. Utekhin, A. N. Lukin, *J. Appl. Phys.* **2005**, *17*, 3457–3463.
- [41] Y. Xie, F. Chen, J. He, J. Zhao, H. Wang, *J. Photochem. Photobiol. A: Chem.* **2000**, *136*, 235–240.
- [42] G. M. Sheldrick, *Acta Crystallogr., Sect. A* **2008**, *64*, 112–122.
- [43] T. Hirai, I. Komasa, *J. Mater. Chem.* **2000**, *10*, 2234–2235.
- [44] A. Y. Satoh, J. E. Trosko, S. J. Masten, *Environ. Sci. Technol.* **2007**, *41*, 2881–2887.

Received: April 14, 2014

Published Online: September 5, 2014